Electronic Supplementary Material (ESI) for Physical Chemistry Chemical Physics.

Supporting Information for:

Insights into the Electrocatalytic Reduction of CO_2 on Metallic Silver Surfaces

Toru Hatsukade, Kendra P. Kuhl, Etosha R. Cave, David N. Abram, and Thomas F. Jaramillo

Department of Chemical Engineering, Stanford University, 381 North-South Mall, Stanford, California 94305,
United States

High Resolution XPS spectrum of Pre- and Post-Run Surfaces

High resolution XPS spectra were taken along with the survey scan shown in the main article. C 1s, O 1s, and Ag MNN peaks are shown here. The spectra are nearly identical between the pre-run and post-run samples, with minor change in the peak intensities of the different Ag oxidation states observed in the Ag MNN spectra. This supports the idea that any changes to the surface observed before and after experimentation are mostly morphological in nature, as seen in the SEM images.

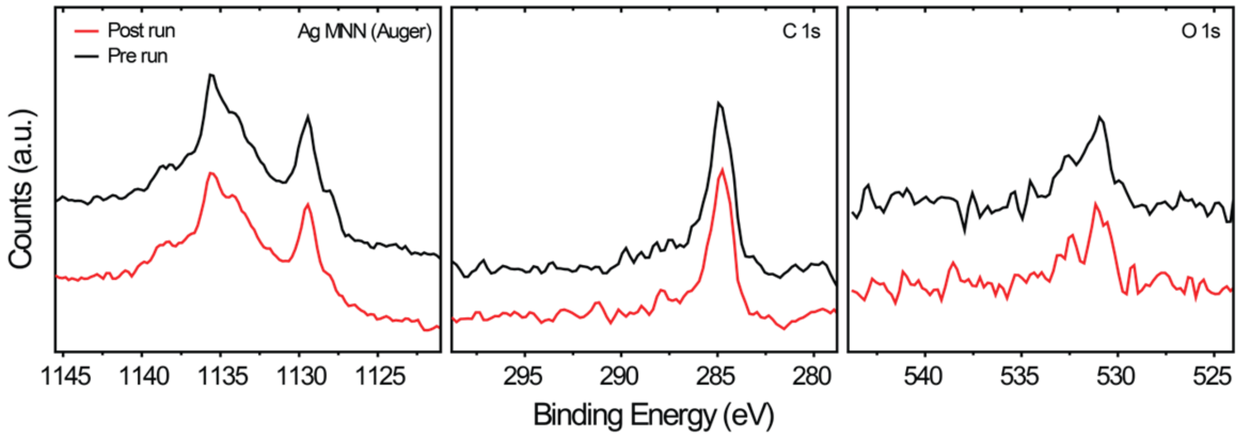

Figure S1. High resolution XPS scans of silver surfaces (—) before and (—) after an hour-long experiment at -1.23 V.

Accuracy of Quantification through Error Bars and Total Faradaic Efficiency

Accurate quantification of each reduction product is crucial in the characterization of electrochemical reduction of CO_2, as it greatly affects the apparent selectivity and activity of the process. Repetition of quantification is a crucial factor, as it allows for the reported values to be more precise. Experiments in this work involved the sampling of the gas phase products four times during each hour-long electrolysis run, and the electrolysis runs were repeated at least three times at each potential. The data shown in the main article is an average of these multiple runs, and precision of the data is expressed here in the form of error bars (Figure S2). The amounts of error in the reported values are noticeable, though it does not have any significant effect on the general trends observed in the selectivity and activity of the reaction.

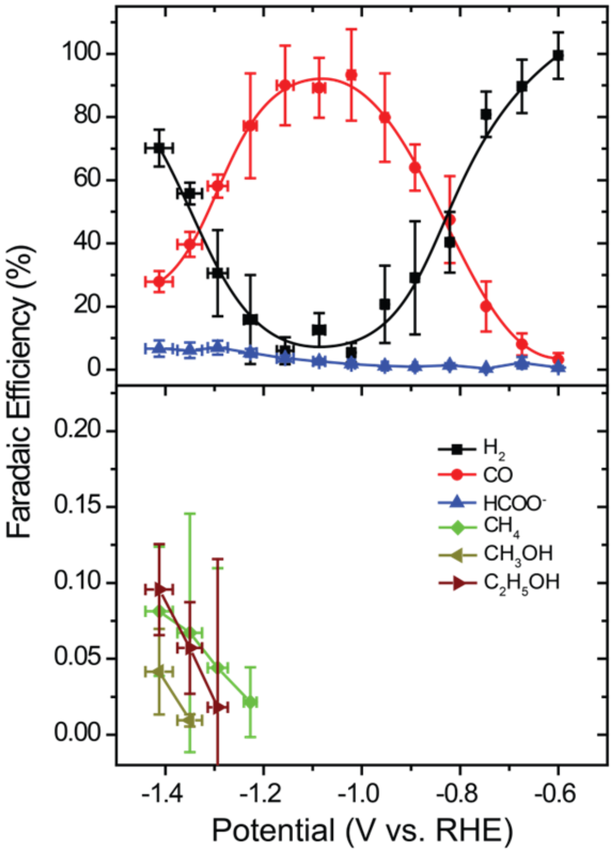

Figure S2. Faradaic efficiency vs. potential with error bars.

The sum of the faradaic efficiency values of reduction products at each potential can be utilized as a measure of the completeness of quantification methods. Since faradaic processes occurring on the silver surface under our operating conditions are likely to produce chemicals that are detectable through our quantification methods, total faradaic efficiency of 100% is expected at each potential. The total faradaic efficiency vs. potential plot (Figure S3) shows most values falling in the range of 95-105%, illustrating the adequacy of the quantification methods. The value at -0.82 V falls outside of this range, having a total faradaic efficiency of ca. 90%. However, 10% error is still within the expected range of experimental error, and it is not detrimental to the overall picture of selectivity and activity gathered from this work.

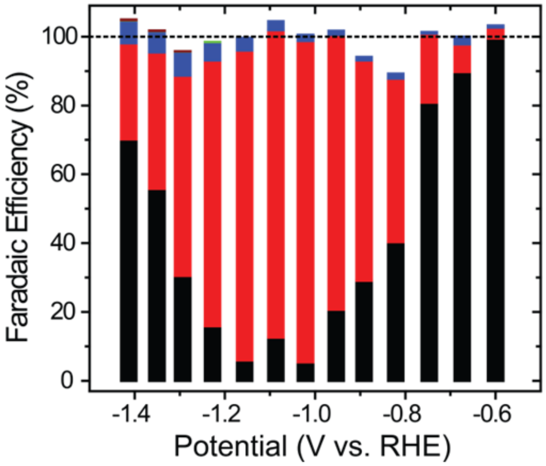

Figure S3. Plot of total faradaic efficiency vs. potential. Black portion of the faradaic efficiency is for hydrogen, red is for CO, blue is for formate, green is for methane, wine is for ethanol, and dark yellow is for methanol. The faradaic efficiencies of the minor products (methane, ethanol and methanol) are most likely overestimated in this depiction, as they contribute to less than 0.1%.

$^{13}CO_2$ labeled NMR spectra

Hour-long electrolysis experiment was performed using ^{13}C-labeled CO_2 in order to identify the origin of the liquid phase products. NMR spectra of the electrolytes from $^{12}CO_2$ and $^{13}CO_2$ experiments are compared in Figure S4, with peaks for formate, methanol, and ethanol presented. The peak splitting of the product peaks due to the coupling of ^{1}H to ^{13}C are well apparent when the spectrums are compared, which confirms that these products originate from CO_2.

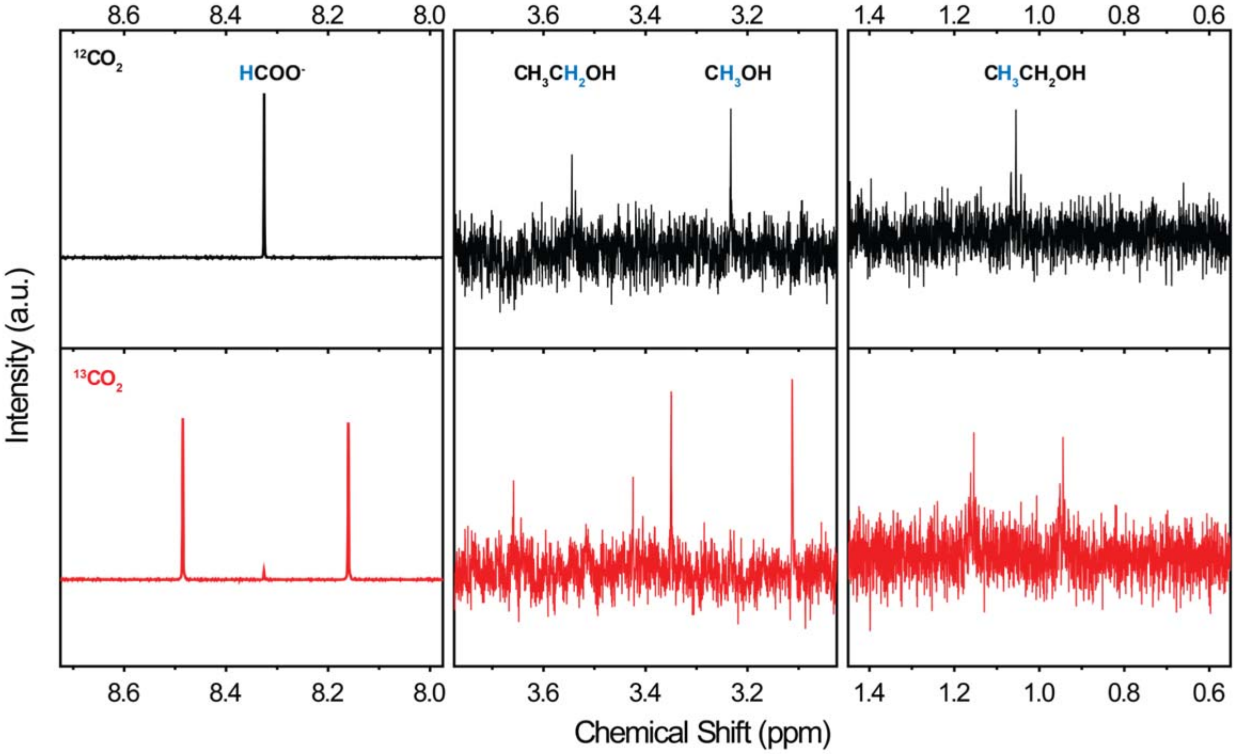

Figure S4. NMR spectrums of the electrolytes from $^{12}CO_2$ and $^{13}CO_2$ experiments. Product peaks for formate, methanol, and ethanol all show ^{13}C splitting.

Mass Transport Limitations

Two additional sets of experiments were performed in order to study possible mass transport limitations. In one case, the concentration of CO_2 in the gas feed was varied while the feed flow rate was kept constant, maintaining a similar mixing profile of the electrolyte (Figure S5a). The other was where the flow rate of pure CO_2 feed was varied (Figure S5b). In both experiments, the current densities measured under varying flow conditions all overlay one another in the low overpotential (kinetically limited) region, showing no dependence on the different flow conditions. Significant differences in current densities, however, were observed in the plateau region among the different flow conditions, suggesting that the CO_2RR is indeed being affected by the mass transport of CO_2 to the catalyst surface at higher overpotentials.

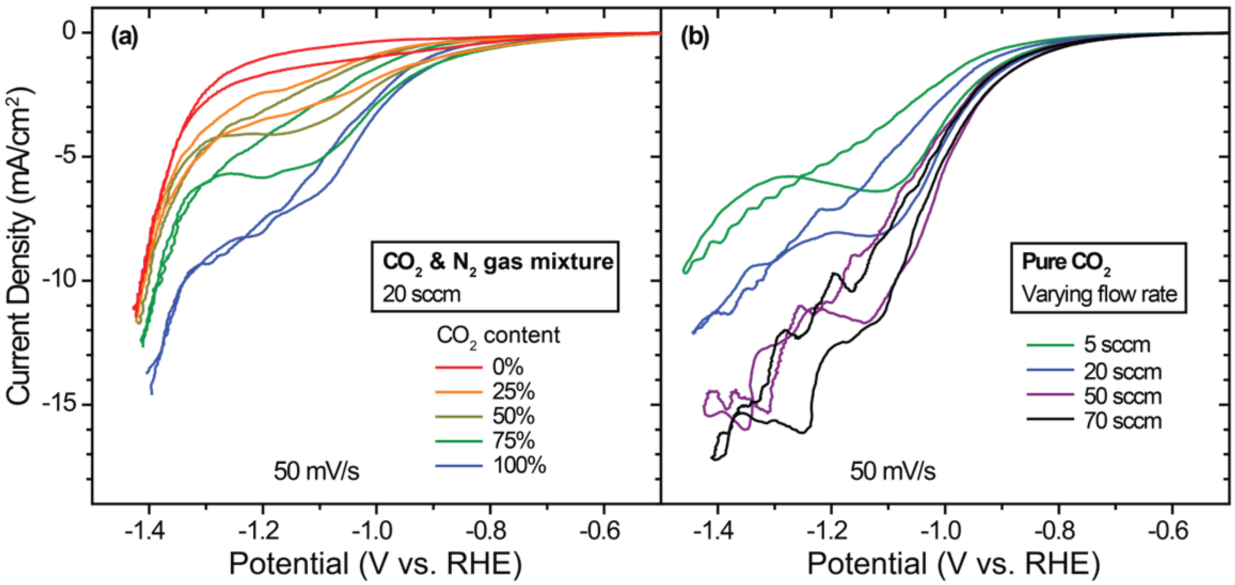

Figure S5. (a) CVs taken under varying CO_2 concentration in the inlet gas stream with a constant flow rate of 20 sccm. (b) CVs taken under varying flow rate of pure CO_2 inlet stream.